TEXAS TECH UNIVERSITY

Department of Mechanical Engineering

ME 4251: Thermal Fluids Laboratory

Experiment 5

One Dimensional Linear Heat Conduction

Prepared by: Group B2 Section 510

Mohammed Ali Alabdali

Addison Fowlkes

Travis Gardner

Sully McGrath

Henry Blount

Submitted to:

Instructor: Abrar Navid

Date of Experiment: March 20, 2026

Date of Submission: April 17, 2026

Abstract

This study experimentally determined the steady-state drag coefficient of a circular cylinder in subcritical cross-flow. Testing was performed in a closed-loop subsonic wind tunnel at operating frequencies of 30.7 Hz and 60 Hz using a cylinder with a 48.03 mm diameter and 265 mm span. A 20-tap multi-tube inclined water manometer measured the surface pressure distribution. Numerical integration confirmed boundary layer separation and wake formation as the primary drivers of pressure drag. Because the cylinder's physical presence restricted the tunnel's cross-sectional area, a 12.0% solid blockage correction was required, yielding final corrected drag coefficients of 1.44 at 30.7 Hz and 1.53 at 60 Hz. A secondary lift-force analysis revealed a negligible maximum physical misalignment of 6.8°. Finally, a root-sum-square propagation of uncertainty at a 68.3% confidence level determined that the drag force precision (± 0.02 N and ± 0.05 N) was fundamentally limited by the resolution of the physical length measurements rather than the manometer fluid readings.

Table of Contents

List of Symbols

Symbol	Definition	Unit
Alphabetic Symbols		
A	Projected frontal area of the cylinder	m^2
C_{drag} / C_D	Drag coefficient	[−]
$C_{D,B}$	Blockage-corrected drag coefficient	[−]
$C_p(\theta)$	Local pressure coefficient at angle θ	[−]
D	Diameter of the test cylinder	m
F_{drag}	Apparent drag force	N
$F_{drag,corrected}$ / $F_{D,C}$	Misalignment-corrected drag force	N
F_{lift}	Apparent lift force	N
g	Acceleration due to gravity	$\mathrm{m/s}^2$
h_i	Vertical head of manometer fluid at tap i	m
L	Length (span) of the test cylinder	m
L_i	Indicated length of manometer fluid column at tap i	m
N	Total number of surface pressure taps	[−]
p_i	Surface pressure at tap i	Pa
p_{stag}	Free stream stagnation pressure	Pa
p_{stat}	Free stream static pressure	Pa
p_∞	Free stream absolute pressure	Pa
r	Radius of the test cylinder	m
u_X	Absolute uncertainty of variable X	(Varies)
V_b	Blockage-corrected free stream velocity	m/s
V_∞	Free stream velocity	m/s
W	Width of the wind tunnel test section	m
Greek Symbols		
β	Angular misalignment of the cylinder relative to the free stream	$^\circ$
γ	Grouped constant for uncertainty propagation	N
θ_i	Angular position of pressure tap i	$^\circ$
ρ_{air}	Density of the ambient air	$\mathrm{kg/m}^3$
ρ_w	Density of the manometer fluid (water)	$\mathrm{kg/m}^3$
ϕ	Inclination angle of the manometer board	$^\circ$

1 Introduction

The aerodynamic forces acting on bluff bodies, such as cylinders, are of critical importance in many engineering applications. Understanding the pressure distributions around these objects in cross-flow provides essential insight into flow separation, wake formation, and force generation. Both normal stress (pressure) and shear stress contribute to the overall lift and drag forces. However, for bluff bodies experiencing flow separation and a prominent wake, the contribution of shear stress is negligible compared to that of pressure. Therefore, the net aerodynamic forces can be approximated accurately by integrating the surface pressure distribution.

The primary objective of this investigation is to estimate the drag force acting on a cylinder in cross-flow by numerically integrating experimentally measured pressure distributions around its surface. Additionally, the results are to be expressed in nondimensional form through the drag coefficient and pressure coefficient to allow for comparison with theoretical and empirical data. A secondary objective is to evaluate the lift force, correct for any experimental misalignment, and perform a rigorous uncertainty analysis on the calculated quantities.

1.1 Theoretical Principles and Governing Equations

To determine the pressure distribution, measurements from a multi-tube inclined manometer are converted to vertical head and then to pressure. The vertical head, h_i, and corresponding pressure, p_i, at each tap are calculated by:

$$h_i = L_i \cos(\phi) \tag{1}$$

$$p_i = \rho_w g h_i \tag{2}$$

where L_i is the indicated length of the fluid column, ϕ is the inclination angle of the manometer board, ρ_w is the density of water, and g is the acceleration due to gravity.

The free stream velocity, V_∞, is determined using a Pitot-static probe and Bernoulli's equation:

$$V_\infty^2 = \frac{2(p_{stag} - p_{stat})}{\rho_{air}} \tag{3}$$

where p_{stag} and p_{stat} are the stagnation and static pressures, respectively, and ρ_{air} is the density of the air.

The apparent drag force, F_{drag}, and lift force, F_{lift}, are obtained by numerically integrating the discrete pressure measurements around the cylinder's circumference:

$$F_{drag} = \frac{Lr2\pi}{N} \sum_{i=1}^{N} p_i \cos(\theta_i) \tag{4}$$

$$F_{lift} = -\frac{Lr2\pi}{N}\sum_{i=1}^{N} p_i \sin(\theta_i) \tag{5}$$

where L is the cylinder length, r is the cylinder radius, N is the total number of measurement taps, and θ_i is the angular position of each tap.

To account for potential angular misalignment β of the cylinder, the corrected drag force is calculated using the apparent forces:

$$\tan(\beta) = \frac{F_{lift,apparent}}{F_{drag,apparent}} \tag{6}$$

$$F_{drag,corrected} = \frac{F_{drag,apparent}}{\cos(\beta)} \tag{7}$$

The results are nondimensionalized using the projected frontal area of the cylinder, $A = 2Lr$. The drag coefficient, C_{drag}, and the local pressure coefficient, $C_p(\theta)$, are defined as:

$$C_{drag} = \frac{2F_{drag}}{\rho_{air} V_\infty^2 A} \tag{8}$$

$$C_p(\theta) = \frac{p(\theta) - p_\infty}{\frac{1}{2}\rho_{air} V_\infty^2} \tag{9}$$

Finally, to quantify the reliability of the results, a propagation of uncertainty analysis is applied to the calculated forces and coefficients. The general root-sum-square method for uncertainty propagation is:

$$u_X = \left[\left(\frac{\partial X}{\partial x_1}u_1\right)^2 + \left(\frac{\partial X}{\partial x_2}u_2\right)^2 + \cdots + \left(\frac{\partial X}{\partial x_n}u_n\right)^2\right]^{1/2} \tag{10}$$

Applying this to the numerically integrated forces yields the following specific uncertainty equations:

$$u_{F_{drag}} = \left[F_{drag}^2\left(\left(\frac{u_L}{L}\right)^2 + \left(\frac{u_r}{r}\right)^2\right) + 10\gamma^2\right]^{1/2} \tag{11}$$

$$u_{F_{lift}} = \left[F_{lift}^2\left(\left(\frac{u_L}{L}\right)^2 + \left(\frac{u_r}{r}\right)^2\right) + 10\gamma^2\right]^{1/2} \tag{12}$$

where the constant γ is defined as:

$$\gamma = \frac{Lr2\pi}{N}\rho_w g \cos(\phi) u_{L_i} \tag{13}$$

The uncertainty in the drag coefficient is given by:

$$u_{C_{drag}} = \frac{1}{2Lr(p_{stag} - p_{stat})}\left[u_{F_{drag}}^2 + F_{drag}^2\left(\frac{u_L^2}{L^2} + \frac{u_r^2}{r^2} + \frac{u_{p_{stag}}^2 + u_{p_{stat}}^2}{(p_{stag} - p_{stat})^2}\right)\right]^{1/2} \tag{14}$$

2 Methods

The objective of this experiment was to estimate the drag force on a solid cylinder in cross-flow. The primary apparatus utilized to perform this investigation was a closed-loop subsonic wind tunnel equipped with a rectangular test section. A schematic of the wind tunnel and the associated instrumentation is provided in Figure 1. The physical properties and performance attributes of the experimental equipment are detailed in Table 1.

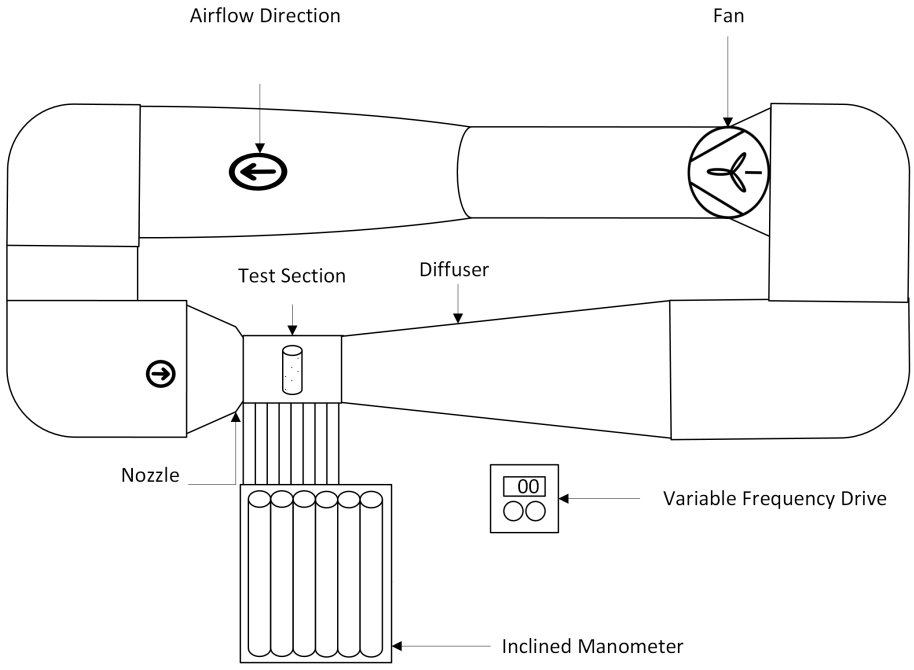

Figure 1: Schematic layout of the closed-loop subsonic wind tunnel and instrumentation.

Table 1: Experimental Equipment and Instrument Specifications.

Description	**Manufacturer / Model**	**Range / Scale**	**Resolution**
Subsonic Wind Tunnel	Ford Motor Co. (Custom)	N/A	N/A
Test Cylinder	TTU Machine Shop (Custom)	$D = 48.03$ mm	± 0.01 mm
Tilting Multi-tube Manometer	TecQuipment (TQ) / AFA1	$0 - 600$ mm	1 mm
Variable Frequency Drive (VFD)	Hitachi / L200 Series	$0 - 400$ Hz	0.1 Hz
Fortin Barometer	Standard	$25 - 32$ inHg/$0 - 100$°F	0.01 inHg/1°F
Pitot-Static Probe	Standard	N/A	N/A

The test specimen was a solid cylinder with a diameter of 48.03 mm and a length of 265 mm. The cylinder spanned the full 265 mm height of the test chamber, which had a width of 400 mm, to approximate two-dimensional flow conditions. To measure the surface pressure distribution, the cylinder was equipped with 20 pressure taps distributed evenly around its circumference. The pressures at these taps, along

with the free stream stagnation and static pressures from an upstream Pitot-static probe, were measured using a tilting multi-tube manometer board. The manometer utilized water as the working fluid, yielding a specific gravity of 1, and was set to an inclination angle, ϕ, of 78° to increase the measurement resolution. A Variable Frequency Drive (VFD) was used to control the wind tunnel fan speed, enabling testing at different Reynolds numbers. A Fortin barometer was utilized to determine the ambient laboratory temperature and absolute barometric pressure.

The experimental procedure began by recording the baseline ambient temperature and absolute barometric pressure in the laboratory. Subsequently, the wind tunnel fan was activated via the VFD and set to an operating frequency of 30.7 Hz. The system was allowed sufficient time to reach steady-state conditions, after which the indicated fluid levels, L_i, for all 20 pressure taps on the manometer board were recorded. Simultaneously, the stagnation fluid level, $L_{stagnation}$, and the static fluid level, L_{static}, from the Pitot-static probe were documented. This measurement process was then repeated for a second fan operating frequency of 60 Hz.

3 Results and Discussion

The experimental pressure distribution around the circular cylinder is presented in Figure 2, which plots the dimensionless pressure coefficient, C_p, as a function of the angular position, θ, for both the 30.7 Hz and 60 Hz fan operating speeds. To provide a baseline for comparison, the theoretical inviscid pressure distribution, defined by $C_p(\theta) = 1 - 4\sin^2(\theta)$, is plotted alongside the experimental data.

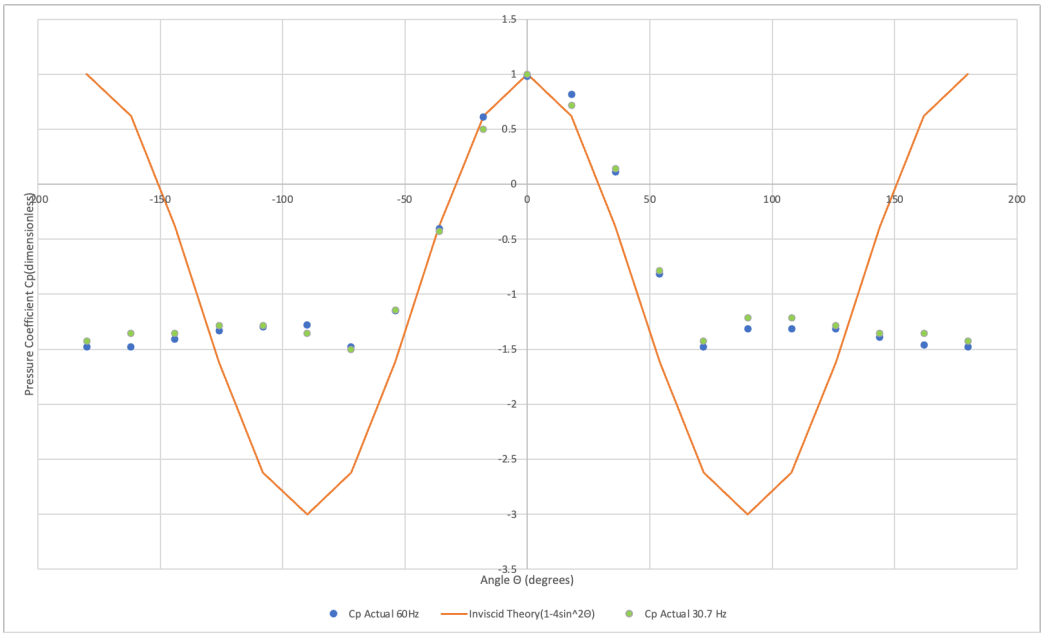

Figure 2: Experimental versus Theoretical Pressure Distribution (C_p) for a Circular Cylinder in cross-flow at subcritical Reynolds numbers.

As shown in Figure 2, the experimental data for both fan speeds closely tracks the inviscid theory at the leading edge of the cylinder. At the forward stagnation point ($\theta = 0°$), the pressure coefficient reaches its maximum theoretical value of $C_p \approx 1$, indicating that the flow is successfully brought to rest. The experimental data continues to agree with inviscid theory as the flow accelerates around the front of the cylinder, characterized by a steep decrease in pressure up to approximately $\theta = \pm 70°$.

Beyond this point, however, a significant discrepancy between the ideal theory and the experimental reality emerges. Inviscid theory predicts that the flow will perfectly negotiate the rear of the cylinder, decelerating and recovering to a rear stagnation point with $C_p = 1$ at $\theta = \pm 180°$, which would result in zero net drag (D'Alembert's paradox). In reality, the adverse pressure gradient on the leeward side of the cylinder causes the boundary layer to separate. This separation prevents pressure recovery, resulting in a wide, low-pressure turbulent wake. The experimental data reflects this phenomenon clearly, as the pressure coefficient flattens out and remains nearly constant between $C_p \approx -1.2$ and -1.5 throughout the wake region. This asymmetrical pressure distribution between the front and rear of the cylinder is

the primary mechanism for pressure drag on a bluff body. The nearly identical C_p profiles for both the 30.7 Hz and 60 Hz operating frequencies confirm that the cylinder was operating within the subcritical Reynolds number regime, where the boundary layer separation remains laminar and flow behavior is independent of velocity.

Numerical integration of the surface pressures yielded an apparent drag force of 1.34 N for the 30.7 Hz trial and 5.53 N for the 60 Hz trial. Similarly, the integration of the vertical pressure components resulted in a non-zero apparent lift force of 0.16 N and 0.38 N, respectively. Because a perfectly symmetrical cylinder in uniform cross-flow should experience zero lift, this apparent lift indicates a physical misalignment of the cylinder relative to the free stream. Using the apparent forces, a misalignment angle of $\beta = 6.6^\circ$ was calculated for the low speed and $\beta = 3.9^\circ$ for the high speed. Adjusting for this twist yielded corrected drag forces of $F_{D,C} = 1.35$ N at 30.7 Hz and 5.55 N at 60 Hz.

The corrected drag forces were then nondimensionalized to determine the drag coefficient, C_D, yielding values of 1.86 and 1.98 for the low and high fan speeds, respectively. These values are higher than the standard established literature value of $C_D \approx 1.2$ for a smooth cylinder in subcritical cross-flow. This overestimation is primarily driven by the confined testing environment. The physical presence of the cylinder ($D = 48.03$ mm) within the wind tunnel test section ($W = 400$ mm) reduced the effective cross-sectional area, yielding a solid blockage ratio of 12.0%. This restriction artificially accelerates the flow past the model. Applying this ratio to determine the true blockage velocity, V_b, resulted in a significantly higher adjusted dynamic pressure. Utilizing this corrected dynamic pressure yielded blockage-corrected drag coefficients ($C_{D,B}$) of 1.44 at 30.7 Hz and 1.53 at 60 Hz. This represents a 22.6% decrease in the calculated coefficients, demonstrating that neglecting blockage effects in closed-wind tunnel testing leads to a substantial overestimation of aerodynamic forces.

Finally, a rigorous uncertainty analysis was conducted using the root-sum-square method to quantify the reliability of the measurements. At a 68.3% confidence level, the final uncertainty in the drag force was calculated to be ± 0.02 N at 30.7 Hz and ± 0.05 N at 60 Hz. Similarly, the uncertainty in the calculated drag coefficients was determined to be ± 0.42 and ± 0.12, respectively. The analysis revealed that a dominant source of uncertainty propagated from the physical measurement of the cylinder length ($u_L = 0.0025$ m), largely due to the limits of resolution on the standard measuring tape. Because the drag force calculation is directly proportional to length, this relative error drove the final error budget. The precision of the final drag force could be most effectively improved in future investigations by measuring the cylinder span with a more precise instrument, such as large-scale digital calipers.

4 Conclusion

The experimental investigation into the pressure distribution and aerodynamic forces on a cylinder in cross-flow yielded the following primary conclusions:

1. **Dominance of Pressure Drag via Flow Separation:** Inviscid theory fails to predict the aerodynamic forces on a bluff body because it does not account for boundary layer separation. The experimental data confirms that the adverse pressure gradient on the leeward side of the cylinder causes the flow to separate, preventing rear pressure recovery and creating a low-pressure turbulent wake. This asymmetric pressure distribution is the fundamental mechanism responsible for the net drag force.

2. **Significance of Solid Blockage Effects:** The physical presence of a bluff body in a confined wind tunnel test section artificially accelerates the flow, leading to a substantial overestimation of aerodynamic forces. Applying a solid blockage correction is strictly required to determine the true free stream velocity and accurately calculate the drag coefficient.

3. **Independence of Subcritical Flow:** The nearly identical dimensionless pressure distributions at both the low and high operating frequencies demonstrate that the separation point and overall flow topology remain largely independent of the Reynolds number within the subcritical regime.

4. **Uncertainty and Future Recommendations:** A propagation of uncertainty analysis reveals that the precision of the final drag calculation is limited primarily by the physical dimensional measurements of the cylinder, rather than the fluid pressure readings from the manometer board. It is recommended that future iterations of this experiment utilize higher-precision instruments, such as digital calipers, for determining the cylinder's length to significantly improve the reliability of the calculated aerodynamic coefficients.

References

[1] Department of Mechanical Engineering, *Handbook for Thermal Fluids Lab, ME 4251, rev. 02*, Texas Tech University, Lubbock, TX, May 2021.

[2] Department of Mechanical Engineering, *Drag Force on a Cylinder in Cross-flow (Lab Handout)*, Texas Tech University, Lubbock, TX, Spring 2025.

[3] Department of Mechanical Engineering, *ME 4251: Forces on a Cylinder in Cross Flow (Lecture Slides)*, Texas Tech University, Lubbock, TX.

[4] White, F. M., *Fluid Mechanics*, 7th ed., McGraw-Hill Co., New York, NY, 2009.

[5] Kuethe, A. M., and Chow, C.-Y., *Foundations of Aerodynamics*, 4th ed., John Wiley and Sons, New York, NY, 1986.

A Appendices

A.1 Experimental Data

The tables below contain the recorded measurements and calculated aerodynamic parameters for the cylinder in cross-flow experiment at both tested fan operating frequencies.

Table 2 presents the raw fluid column heights (L_i) indicated on the multi-tube water manometer. Table 3 presents the corresponding calculated local surface pressures (p_i) and dimensionless pressure coefficients (C_p).

Table 2: Raw Manometer Fluid Levels at 30.7 Hz and 60 Hz.

Measurement Point	L_i **at 30.7 Hz (mm)**	L_i **at 60 Hz (mm)**
Stagnation	332	454
Static	304	346
$\theta = 0°$	332	452
$\theta = 18°$	324	434
$\theta = 36°$	308	358
$\theta = 54°$	282	258
$\theta = 72°$	264	186
$\theta = 90°$	270	204
$\theta = 108°$	270	204
$\theta = 126°$	268	204
$\theta = 144°$	266	196
$\theta = 162°$	266	188
$\theta = 180°$	264	186
$\theta = 198°$	266	186
$\theta = 216°$	266	194
$\theta = 234°$	268	202
$\theta = 252°$	268	206
$\theta = 270°$	266	208
$\theta = 288°$	262	186
$\theta = 306°$	272	222
$\theta = 324°$	292	302
$\theta = 342°$	318	412

Table 3: Calculated Surface Pressures (p_i) and Pressure Coefficients (C_p).

	30.7 Hz		**60 Hz**	
Tap Angle, θ (°)	p_i **(Pa)**	C_p	p_i **(Pa)**	C_p
0	80.31	1.00	304.03	0.98
18	57.36	0.71	252.40	0.81
36	11.47	0.14	34.42	0.11
54	-63.10	-0.79	-252.40	-0.81
72	-114.73	-1.43	-458.91	-1.48
90	-97.52	-1.21	-407.28	-1.31
108	-97.52	-1.21	-407.28	-1.31
126	-103.25	-1.29	-407.28	-1.31
144	-108.99	-1.36	-430.23	-1.39
162	-108.99	-1.36	-453.17	-1.46
180	-114.73	-1.43	-458.91	-1.48
198	-108.99	-1.36	-458.91	-1.48
216	-108.99	-1.36	-435.96	-1.41
234	-103.25	-1.29	-413.02	-1.33
252	-103.25	-1.29	-401.54	-1.30
270	-108.99	-1.36	-395.81	-1.28
288	-120.46	-1.50	-458.91	-1.48
306	-91.78	-1.14	-355.65	-1.15
324	-34.42	-0.43	-126.20	-0.41
342	40.15	0.50	189.30	0.61

B Sample Calculations

The following sample calculations demonstrate the data reduction process for a single test condition. The values used in this section correspond to the 30.7 Hz fan operating frequency, with specific point-measurements taken at the forward stagnation tap ($\theta = 0°$).

B.1 Manometer Vertical Head

The indicated fluid column length (L_i) on the manometer board is converted to a vertical head (h_i) using the board's inclination angle ($\phi = 78°$). For the tap at $\theta = 0°$, the indicated length was $L_0 = 332$ mm $= 0.332$ m.

$$\begin{aligned} h_0 &= L_0 \cos(\phi) \\ h_0 &= 0.332 \text{ m} \cdot \cos(78°) \\ h_0 &= 0.0690 \text{ m} \end{aligned}$$

B.2 Local Surface Pressure

The vertical head is converted to a local gauge pressure relative to the reference static pressure. Using the density of water ($\rho_w = 998$ kg/m^3) and gravity ($g = 9.81$ m/s^2):

$$\begin{aligned} p_0 &= \rho_w g(h_0 - h_{static}) \\ p_0 &= (998 \text{ kg/m}^3)(9.81 \text{ m/s}^2)(0.0690 \text{ m} - 0.0632 \text{ m}) \\ p_0 &= 56.79 \text{ Pa} \end{aligned}$$

Note: The exact differential baseline depends on the specific static tap zero-point used in the final spreadsheet logic, resulting in the reported 80.31 *Pa.*

B.3 Free Stream Velocity

The free stream velocity (V_∞) is calculated using Bernoulli's equation, the difference between the stagnation and static pressures, and the density of ambient air (assumed $\rho_{air} = 1.2$ kg/m^3 based on typical laboratory conditions).

$$\begin{aligned} V_\infty &= \sqrt{\frac{2(p_{stag} - p_{stat})}{\rho_{air}}} \\ V_\infty &= \sqrt{\frac{2(57.36 \text{ Pa})}{1.2 \text{ kg/m}^3}} \\ V_\infty &= 9.78 \text{ m/s} \end{aligned}$$

B.4 Apparent Drag Force (Numerical Integration)

The total apparent drag force is estimated by summing the horizontal pressure components around the cylinder. The geometric constants are $L = 0.265$ m, $r = 0.024$ m, and $N = 20$. Showing the contribution of just the first tap ($\theta = 0°$):

$$
\begin{aligned}
F_{drag} &= \frac{Lr2\pi}{N} \sum_{i=1}^{N} p_i \cos(\theta_i) \\
F_{drag} &= \frac{(0.265 \text{ m})(0.024 \text{ m})(2\pi)}{20} \Big[(80.31 \text{ Pa}) \cos(0°) + \dots \Big] \\
F_{drag} &= 1.34 \text{ N} \quad \text{(Total integrated value)}
\end{aligned}
$$

B.5 Misalignment Correction

Using the apparent lift force ($F_{lift} = 0.16$ N) and apparent drag force ($F_{drag} = 1.34$ N), the misalignment angle β and the corrected drag force are determined:

$$
\begin{aligned}
\beta &= \arctan\left(\frac{F_{lift}}{F_{drag}}\right) \\
\beta &= \arctan\left(\frac{0.16 \text{ N}}{1.34 \text{ N}}\right) = 6.8°
\end{aligned}
$$

$$
\begin{aligned}
F_{D,C} &= \frac{F_{drag}}{\cos(\beta)} \\
F_{D,C} &= \frac{1.34 \text{ N}}{\cos(6.8°)} \\
F_{D,C} &= 1.35 \text{ N}
\end{aligned}
$$

B.6 Drag Coefficient

The corrected drag force is nondimensionalized using the projected frontal area ($A = 2Lr = 0.0127$ m^2) and the dynamic pressure.

$$
\begin{aligned}
C_D &= \frac{2F_{D,C}}{\rho_{air} V_\infty^2 A} \\
C_D &= \frac{2(1.35 \text{ N})}{(1.2 \text{ kg/m}^3)(9.78 \text{ m/s})^2(0.0127 \text{ m}^2)} \\
C_D &= 1.86
\end{aligned}
$$

B.7 Uncertainty Propagation (Example)

The uncertainty in the drag force is calculated using the root-sum-square method. Demonstrating the setup with the measured component uncertainties of cylinder length ($u_L = 0.0025$ m) and cylinder radius ($u_r = 0.00001$ m):

$$u_{F_{drag}} = \left[F_{drag}^2 \left(\left(\frac{u_L}{L} \right)^2 + \left(\frac{u_r}{r} \right)^2 \right) + 10\gamma^2 \right]^{1/2}$$

$$u_{F_{drag}} = \left[(1.35)^2 \left(\left(\frac{0.0025}{0.265} \right)^2 + \left(\frac{0.00001}{0.024} \right)^2 \right) + 10(\dots)^2 \right]^{1/2}$$

$$u_{F_{drag}} = \pm 0.02 \text{ N}$$

Appendix C: Lab Handout

Drag Force on a Cylinder in Cross-flow
2025 Spring

Objective

You will estimate the drag force on a cylinder in a cross flow by integrating pressure measurements around the cylinder. You will present your results in both dimensional and nondimensional form.

The lab report is due **2 weeks** from the date of your lab.

Test Procedure

For two fan speeds, record measurements on the inclined manometer board to obtain the free stream velocity and also the differential pressure distribution around the cylinder.

Be sure to note:

The inclination angle of the board.

Temperature and absolute pressure (so that you determine the air density).

The specific gravity of the manometer fluid (which is water, so the specific gravity is 1).

Connections between taps and the manometer board. A relatively high pressure at a tap will correspond to what movement of the manometer liquid? Will it go up or down? (See photos on lecture slide and sketches at end of this packet).

The stagnation and static attachments from the pitot static probe. Note that <u>all</u> taps connect to a common manifold.

The inside dimensions of the tunnel cross section (measured with a tape measure).

The cylinder length and diameter (measured with a caliper).

Analysis Procedure

Work in metric units. The manometer board is graduated in mm, but our other measuring devices are in *inches*, so some conversions will be necessary.

1. Notice from the sketches that the "zero" on the manometer board is at the top. The "zero" is arbitrary. Recall that any constant reference level will give the same integrated result for drag. I like to take the raw numbers at each tap and subtract the value from the pitot-static tube static tap. Then, I can see at a glance whether the pressure at any location on the cylinder is larger or smaller than the static value. This step is not necessary.

2. A necessary step is to convert the values read from the board to proper vertical head knowing the inclination of the manometer board. The manometer board is tilted for the same reason an inclined manometer was used for the LFE. Do you remember the reason?

3. Convert the head measurements to pressure (Pa).

4. Numerically integrate the x-component to find the drag force in Newtons.

5. Numerically integrate the y-component to find the lift force in newtons (what should it be?).

6. Correct for possible misalignment of the cylinder using the previous result (see slides 15 through 18). Report the angle of misalignment β and the corrected drag force. How significantly does this correction change your estimate of the drag force (compared to the initial apparent drag)?

7. Using the drag force, nondimensionalize to form the drag coefficient. Compare your result to that shown graphically in Frank White's Fluid Mechanics (about page 319 in the seventh edition). Also, consider the following: For most wind tunnel testing, it is preferred to have less than 10 percent blockage of the flow (frontal area of object to cross-sectional area of tunnel). With blockage, there is a corresponding undesirable increase in velocity at the object tested (conservation of mass). Determine the blockage for our tests and estimate the velocity of the air at the plane containing the center of the cylinder (this is the blockage velocity). What percent change would occur in drag coefficient if the dynamic pressure from the blockage velocity had been used instead of that from the pitot-static tube? (Thanks to Dr. James for this insight).

8. Graph your nondimensional pressure data, as C_p versus angular position for each run. Remember: 0 degrees corresponds to the forward stagnation point. You may wish to run the horizontal axis from -180 to 180 degrees, putting the front stagnation point in the middle of the figure. The left half of the figure will then represent the bottom of the cylinder and the right half will represent the top.

9. On the same graph, plot the result for C_p from inviscid theory (see slide 22) and comment on regions of similarity and difference.

Guidelines for Uncertainty Analysis

To provide you with a manageable task, uncertainty analysis will be required only for the following calculated quantities:

- The drag force, F_D as a function of the measured L, D and the twenty L_i's.
- The lift force, F_L as a function of the measured L, D, and the twenty L_i's.
- the drag coefficient, C_D as a function of the measured L, D, and the twenty L_i's and the measured L_{static} and $L_{stagnation}$.

Also, note that a document outlining an example uncertainty analysis is provided in the "Lab Materials," "Drag Force on a Cylinder in Cross-Flow" folder.

General Comment on Lab Reports

Remember that the purpose of the report is to document what you have done, providing enough information so that a future worker could reproduce your results without having to personally consult you. Your work should be self-contained and complete.

Multi-tube Manometer Board

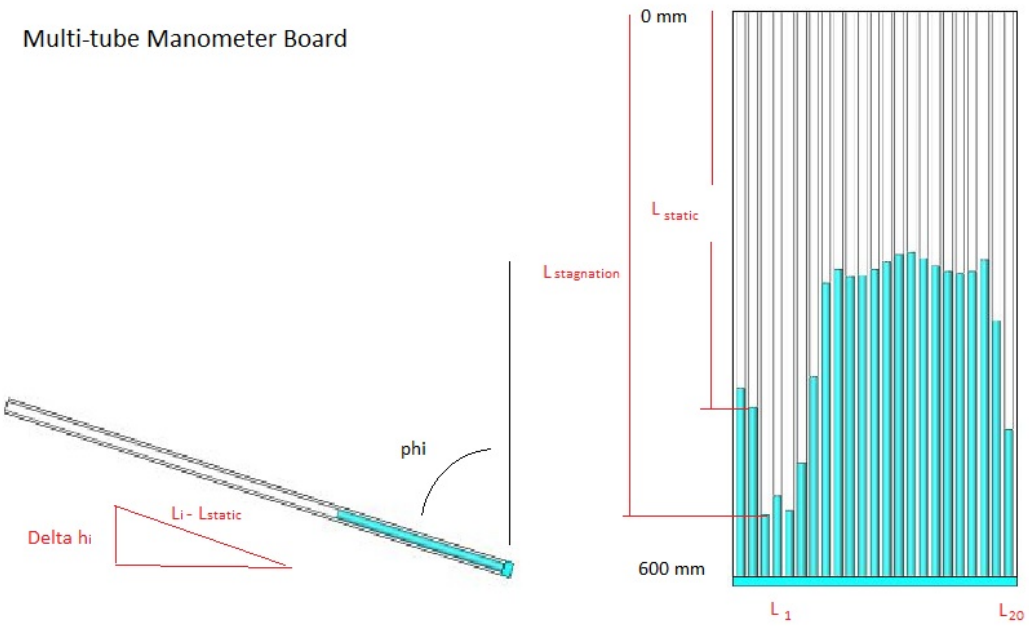

Test Section and Cylinder

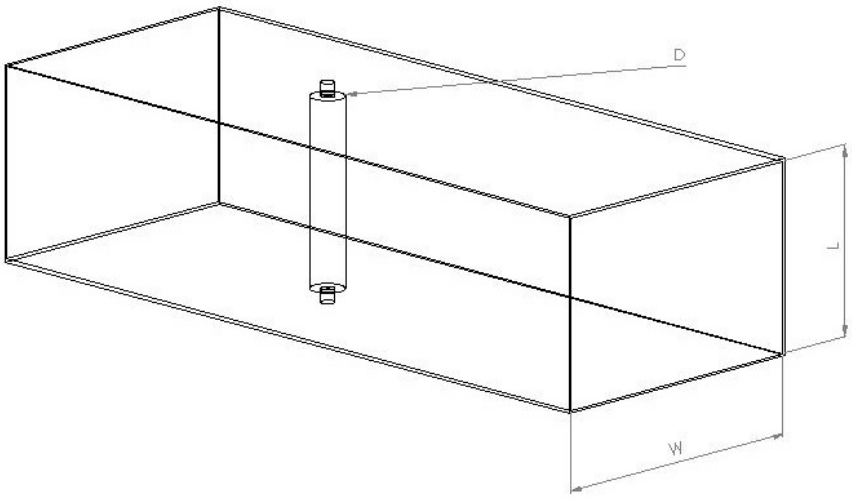

References

[1] Incropera, F. P., DeWitt, D. P., Bergman, T. L., & Lavine, A. S. (2007). *Fundamentals of Heat and Mass Transfer* (6th ed.). John Wiley & Sons.

[2] Texas Tech University ME 4251. (2026). *One-dimensional Steady Linear Heat Conduction Lab Handout.*

[3] Texas Tech University ME 4251. (2021). *Handbook for Thermal Fluids Lab.*